# Simulation of pesticide transport in 70-m-thick soil profiles in response to large water applications

Tiantian Zhou[a,*], Giuseppe Brunetti[b], Nels Ruud[c], Jiří Šimůnek[d], Wenyi Cui[a], Anran Liao[e], Paolo Nasta[f], Jiaxin Gao[g], Elad Levintal[h], Cristina Prieto García[a], Helen E. Dahlke[a,*]

a Department of Land, Air and Water Resources, University of California, Davis, CA, 95616, USA
b Department of Civil Engineering, University of Calabria, Rende, Italy
c Department of Pesticide Regulation, California Environmental Protection Agency, Sacramento, CA, USA
d Department of Environmental Sciences, University of California, Riverside, CA, 92521, USA
e School of Environment, Tsinghua University, Beijing 100084, China
f Department of Agricultural Sciences, AFBE Division, University of Naples Federico II, Portici (Naples), Italy
g Department of Chemistry, University of California, Riverside, CA, 92521, USA
h Zuckerberg Institute for Water Research, The Jacob Blaustein Institutes for Desert Research, Ben-Gurion University of the Negev, Sde Boker campus, 84990, Israel

## Abstract

Global groundwater depletion is a pressing issue, particularly in regions dependent on groundwater for agriculture. Agricultural Managed Aquifer Recharge (Ag-MAR), where farm fields are used as spreading grounds for flood water, is a promising strategy to replenish groundwater, but it raises concerns about pesticide leaching into aquifers, posing risks to both drinking water quality and ecosystems. This study employs a physically based unsaturated flow model, a Bayesian probabilistic approach and novel towed transient electromagnetic (tTEM) data to determine the fate and transport, especially the maximum transport depths (MTDs) of four pesticide residues (*Imidacloprid*, *Thiamethoxam*, *Chlorantraniliprole*, and *Methoxyfenozide*) in three 70-m-thick unsaturated zones (P1, P2, P3) of California's Central Valley alluvial aquifer. The results show that Ag-MAR significantly increased MTDs across all profiles for all pesticides and with higher variability in pesticide transport depths compared to the natural rainfall scenario. Profile P2, with the highest sand content exhibited the deepest MTDs under Ag-MAR, indicating a strong influence of soil texture on pesticide transport. While natural capillary barriers at the depth of 2.5-20 m impede water flow under natural rainfall conditions, the high-pressure infiltration during Ag-MAR overcomes these barriers, leading to deeper water and pesticide movement. Among various evaluated pesticides, *Methoxyfenozide* exhibited the smallest absolute MTDs but the largest relative increases in MTDs (RMTDs) under Ag-MAR due to its persistence and low mobility, posing a higher risk of deep transport during intensive recharge events. In contrast, *Thiamethoxam* showed the largest MTDs under both scenarios but smaller RMTDs due to its high mobility, suggesting a more consistent transport behavior regardless of recharge practices. The findings highlight the importance of understanding both site-specific and pesticide-specific behaviors to mitigate groundwater contamination risks during large water applications.

**Keywords:** Towed transient electromagnetic system; Bayesian probabilistic approach; Soil water; Pesticide transport and fates; Capillary barrier; Groundwater pollution

# 1 Introduction

Global groundwater depletion has become a significant concern worldwide and is particularly acute in areas reliant on groundwater for agricultural irrigation (Gleeson et al., 2012). Managed Aquifer Recharge (MAR), defined as the purposeful recharge of water to aquifers for subsequent recovery or environmental benefit (Dillon et al., 2009), is increasingly used to counter groundwater depletion. With the acceleration in global groundwater depletion rates (Dillon et al., 2019; Konikow, 2011), there is a growing need to implement MAR to maintain, enhance, and secure stressed groundwater aquifers. Permeable soils make ideal locations for managed aquifer recharge. More spreading areas need to be employed to grow MAR beyond its estimated current use of 10 $km^3$/year (Dillon et al., 2019), making agricultural land an ideal candidate because of its connection to water conveyance infrastructure that could deliver source water (Levintal et al., 2023). When flood water is intentionally diverted onto farm fields for recharge, a method known as Agricultural Managed Aquifer Recharge (Ag-MAR), concerns about the potential leaching of pesticides through the soil profile into aquifers, leading to exacerbated drinking water and environmental issues (Levintal et al., 2023), need to be raised.

Pesticide use in agriculture has remained globally at about 2.7 million tons of active ingredients annually since 2020, with a significant portion utilized in the USA, Brazil, and China (FAO, 2021). Many studies show that soil pesticides may have detrimental side effects on soil ecosystems by affecting soil biochemical properties and soil food webs (Riah et al., 2014). This disruption can lead to a decline in beneficial soil organisms contributing to nutrient (such as nitrate) cycling, soil health, and greenhouse gas emissions (Sim et al., 2022). On the other hand, pesticides have been identified as a growing threat to drinking water wells in the United States, with 41% of sampled wells showing pesticide compounds and their metabolites (Bexfield et al., 2021). Most pesticides are found in shallow, unconfined wells extracting modern-age groundwater, suggesting that recharge from rainfall or irrigation facilitates pesticide transport to groundwater, especially in regions where soils are more permeable (Bexfield et al., 2021). Detailed knowledge of water flow and pesticide fate and transport in the unsaturated zone (i.e., a buffer zone that separates the land surface where pesticides are applied from the groundwater aquifer) is needed to address these issues.



3

Pesticide transport in the unsaturated zone is influenced by soil depth and layering, crop characteristics, and various physical and biochemical processes such as precipitation, irrigation, evapotranspiration, surface runoff, drainage, adsorption to particles, and degradation. Other processes, such as volatilization and crop uptake, also play a role but are less important (Köhne et al., 2009). On the other hand, preferential flow and transport (a.k.a. physical/chemical nonequilibrium), often difficult to observe at the point scale (Vogel, 2019), makes it more challenging to quantify pesticide fate and transport and its potential groundwater contamination risk (Jarvis, 2007). These physical and biochemical processes are often studied through the combined use of experimental data and numerical models (la Cecilia et al., 2021).

Numerical flow and transport modeling requires the knowledge of soil hydraulic and solute transport parameters characterized by strong spatial heterogeneity. In the shallow unsaturated zone, these parameters are typically acquired through inverse modeling by minimizing discrepancies between readily measured state variables and fluxes and their corresponding model simulations (Šimůnek and Hopmans, 2002). However, inverse modeling becomes less feasible for deep unsaturated zones due to limited measurements of state variables and fluxes at deeper depths. Nevertheless, with the rapid decline in groundwater levels (Jasechko et al., 2024), there is also interest in recharging the deep unsaturated zone. Consequently, when evaluating the appropriateness of a deep unsaturated zone for Ag-MAR, it is imperative to have detailed information regarding the deep subsurface materials and their hydraulic attributes (Behroozmand et al., 2019).

Laboratory soil texture analysis on soil cores provides accurate results with high vertical resolution but is inefficient and thus limited to the shallow unsaturated zone. In contrast, near-surface geophysical methods (such as the towed transient electromagnetic (tTEM) system) have become increasingly popular due to their ability to offer cost-effective, high-resolution imaging of subsurface structures, which offers a



4

promising tool for understanding the deep unsaturated zone processes (Perzan et al., 2023). While some emerging research has combined tTEM data and unsaturated zone modeling to characterize groundwater recharge efficiency (Pepin et al., 2022; Perzan et al., 2023), little has focused on the pesticide fate and transport under Ag-MAR, especially for a deep unsaturated zone. On the other hand, the interpretation of the electric resistivity acquired by tTEM often results only in a binary classification of fine and coarse-textured sediments (Pepin et al., 2022). It thus produces great uncertainty when used to predict the deep unsaturated zone processes.

In this study, we combine field observations and HYDRUS-1D numerical modeling approaches to analyze the fate and transport of four common pesticides (*Imidacloprid*, *Thiamethoxam*, *Chlorantraniliprole*, and *Methoxyfenozide*) in the deep unsaturated zone (about 70 m) of three Ag-MAR sites in the Central Valley, California. This research builds on the earlier work by (Zhou et al., 2024), which focused on the shallow vadose zone (0–2.5 m), by extending the analysis to focus specifically onto the deeper vadose zone (0–70 m). Key innovations in this study include applying Bayesian probabilistic methods to improve parameter estimation and uncertainty quantification and leveraging towed transient electromagnetic (tTEM) data to assess the impact of deep vadose zone heterogeneity. A significant advancement also includes evaluating pesticide transport under both Ag-MAR practices and natural rainfall conditions while considering a wide range of soil texture permutations across multiple vadose zone layers. These advancements address critical knowledge gaps by providing a comprehensive risk evaluation of pesticide transport across deep unsaturated zones, thereby offering practical insights for sustainable Ag-MAR management.

The objectives of this study are to 1) assess the predictive accuracy and uncertainty of the HYDRUS-1D model using a Bayesian probabilistic approach, 2) analyze parameter sensitivity and how it is connected to dominant processes and factors governing water flow and pesticide transport, 3) quantify the impacts of unsaturated zone heterogeneity on water and pesticides mass balance and water travel times, and 4) evaluate the maximum transport depths of pesticides and potential groundwater contamination risks in response to Ag-MAR by testing all possible permutations of tTEM soil texture data.

# 2 Materials and Methodology

## 2.1 Study site and experimental setup

The Ag-MAR experiment was conducted at Terranova Ranch in the Kings River basin, California, on a 32,376 m² recharge plot (Fig. 1a). The plot was continuously flooded with 38,774 m³ (1.2 m in depth) of groundwater at a flow rate of ~3.35 $m^3$/min between February 16 and 24, 2021. We selected three soil profiles (P1, P2, P3) to study water flow and pesticide transport under Ag-MAR (Fig. 1b). Before flooding, 541 g of $Br^-$ (equivalent to 806 g of KBr) dissolved in 100 L of water was applied at a concentration of 5410 ppm over a 2.5 × 7 m² area at each profile. The application occurred on February 15, 2021, at P1 and P2, and on February 16, 2021, at P3 with an irrigation rate of 0.00381 cm/min.

Soil samples were taken at 15 cm intervals down to 2.5 m before and after flooding. Soil texture analysis of the shallow 2.5 m zone across the three selected soil profiles revealed increasing sand fractions from P1 (41%), P3 (61%), to P2 (84%) (Fig. 1b; Table S1), and a cemented duripan layer at around 1 m depth at P1 and P3. Towed transient electromagnetic (tTEM) data collected in September 2019 provided a description of subsurface sediment materials down to 70 m (the groundwater table depth during the experiment), distinguishing fine and coarse textures (Fig. S1, Table S2). More information on the derivation of sediment texture from tTEM data can be found in (Goebel and Knight, 2021).

Meteorological data, including precipitation and potential evaporation (Fig. S3), were collected at the site, and sensors were installed in each profile at depths of 0.2, 0.6, 1.0, and 2.5 m to monitor soil moisture and ponding levels throughout the flooding period at a 10-minute time interval. Suction cups installed at depths of 0.2, 0.6, 1.0, 1.75, and 2.5 m at each profile collected breakthrough curve data for bromide and residual pesticides, with sampling conducted every 4 hours during the flooding period (Fig. 1c). The suction cups were placed about 50 cm apart, within a maximum horizontal distance of 3.5 meters from the sensor profile.

The California Department of Food and Agriculture analyzed the soil pore water samples collected during the experiment for 54 pesticide compounds using four methods: GWPP Multi-Analyte Screen, Triazine Screen, DCPA Screen, and SWPP Multi-Analyte Screen. The analysis detected thirteen residual pesticide compounds at concentrations above trace levels, including azoxystrobin, *Imidacloprid*, *Mefenoxam/Metalaxyl*, *Metolachlor*, *Simazine*, *Thiamethoxam*, *Methoxyfenozide*, *Chlorantraniliprole*, *Propiconazole*, and *Clomazone* (Tables S3-S4). However, only *Imidacloprid*, *Thiamethoxam*, *Methoxyfenozide*, and *Chlorantraniliprole* had consistent observations throughout the study. None of the four pesticides were detected in groundwater.

The application history (e.g., the application date, crop type, product name, active ingredient concentration, application rate, area treated, and the total amount applied) and key physical and chemical properties of these four pesticides are detailed in Tables S2-S3 of (Zhou et al., 2024). The most recent application dates were June 4, 2020, for *Imidacloprid* (8.5 months before the Ag-MAR experiment), July 11, 2020, for both *Thiamethoxam* and *Chlorantraniliprole* (7 months prior to the experiment), and September 24, 2018, for *Methoxyfenozide* (29 months before the experiment).



7

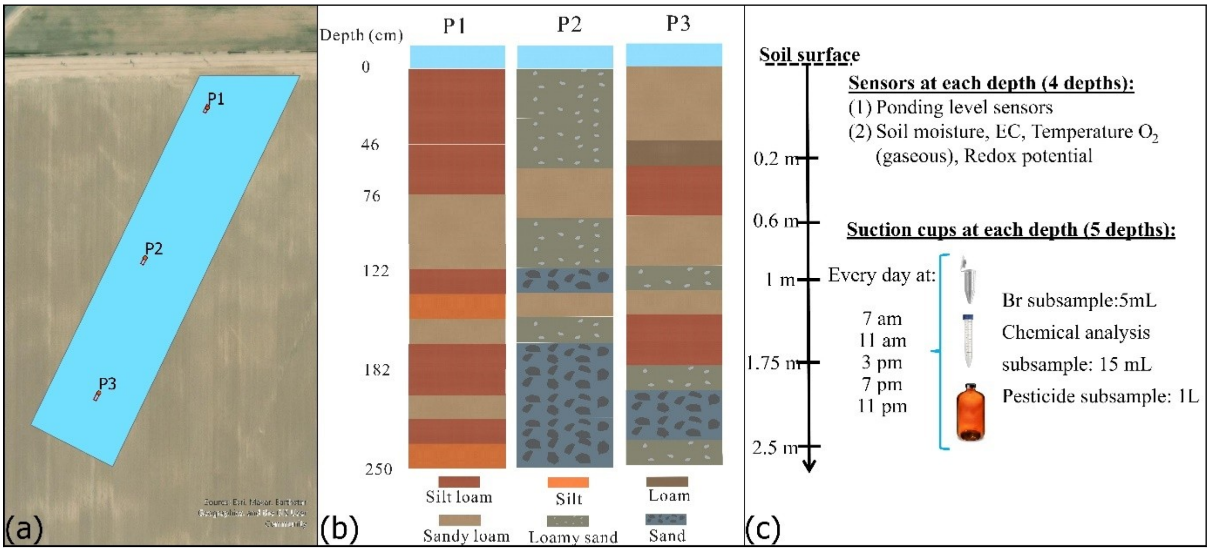


Figure 1. Location of the recharge plot and three soil profiles P1, P2, and P3 (a), the soil texture at each profile (b), and sampling details (c).

## 2.2 HYDRUS-1D model setup

Water flow, bromide (KBr), and pesticide transport in the unsaturated zone were simulated using the HYDRUS-1D software, which solves the Richards equation for water flow and the advection-dispersion equation for solute transport based on certain initial and boundary conditions (Šimůnek et al., 2024; Šimůnek et al., 2016). The governing flow and transport equations are solved numerically using Galerkin-type linear finite element schemes. The mixed form of the Richards equation is solved using the mass-conservative method proposed by (Celia et al., 1990), which has become a standard method in most vadose zone codes. This scheme is highly mass conservative, conserving the mass not only in homogeneous, but also in heterogeneous transport domains. Similarly, the Galerkin-type linear finite element scheme is used to solve the convection-dispersion equation for solute transport. No special measures need to be taken in these Galerkin-type linear finite element schemes to maintain mass continuity for both flow and transport when crossing the boundaries of distinct soil layers. Additionally, HYDRUS-1D evaluates the mass balance errors for both water flow and



8

solute transport at each time step. The mass balance errors reported by the code were typically significantly lower than 0.1% for water flow and 1% for solute transport.

### 2.2.1 Governing equations

The one-dimensional movement of soil water can be described using the Richards equation:

$$\frac{\partial\theta(h)}{\partial t}=\frac{\partial}{\partial z}\left[K(h)\left(\frac{\partial h}{\partial z}+1\right)\right] \tag{1}$$

where $\theta$ represents the volumetric water content [$L^3L^{-3}$], $t$ is time [T], $h$ denotes the water pressure head [L], $z$ is the vertical spatial coordinate [L] with a positive direction upwards, and $K$ refers to the hydraulic conductivity [$LT^{-1}$]. The soil's hydraulic properties, including water retention and hydraulic conductivity, are modeled using the van Genuchten-Mualem (VGM) equations (Mualem, 1976; van Genuchten, 1980):

$$\theta(h)=\begin{cases}\theta_r+\dfrac{\theta_s-\theta_r}{[1+|\alpha h|^n]^m} & h<0\\ \theta_s & h\geq 0\end{cases} \tag{2}$$

$$K(h)=K_s S_e^l ¿ \tag{3}$$

$$S_e=\frac{\theta-\theta_r}{\theta_s-\theta_r} \tag{4}$$

$$m=1-1/n \quad (n>1) \tag{5}$$

where $\theta_r$ and $\theta_s$ are the residual and saturated water contents [$L^3L^{-3}$], respectively; $K_s$ denotes the saturated hydraulic conductivity [$LT^{-1}$]; $S_e$ is the effective saturation [-]; $l$ is the pore connectivity parameter (commonly set to 0.5); $n$ is a shape parameter related to the pore-size distribution [-]; and $\alpha$ is an air-entry suction parameter [$L^{-1}$].

Solute transport in the vadose zone is described using the advection-dispersion equation:



9

$$\frac{\partial \theta C}{\partial t}+\rho\frac{\partial s}{\partial t}=\frac{\partial}{\partial z}\left(\theta D\frac{\partial C}{\partial z}\right)-\frac{\partial (qC)}{\partial z}-\phi \tag{6}$$

where $C$ is the solute concentration in the liquid phase [$ML^{-3}$], $\rho$ is the soil bulk density [$ML^{-3}$], $s$ is the sorbed concentration on soil particles [$MM^{-1}$], $q$ is the water flux [$LT^{-1}$], $D$ is the effective dispersion coefficient [$L^2T^{-1}$], and $\phi$ is a sink term representing degradation reactions [$ML^{-3}T^{-1}$].

The absorbed concentration $s$ is modeled using the Freundlich adsorption isotherm, expressed as:

$$s=K_d C^{\eta} \tag{7}$$

where $K_d$ is the distribution coefficient between liquid and solid phases [$L^3M^{-1}$], and $\eta$ is the Freundlich exponent [-], which was set to 1 in this study for linear adsorption. The effective dispersion coefficient $D$ combines both molecular diffusion and mechanical dispersion:

$$D=\lambda v+\frac{D_0\tau}{\theta} \tag{8}$$

where $\lambda$ is the dispersivity [L], $v$ is the pore-water velocity [$LT^{-1}$], $D_0$ is the molecular diffusion coefficient [$L^2T^{-1}$], and $\tau$ is the tortuosity factor [-]. For bromide, $D_0$ is about 1.584 $cm^2$/d for $Br^-$ (Isch et al., 2019; Köhne et al., 2004), while for pesticides, it is about 0.43 $cm^2$/d (Dusek et al., 2015).

The degradation sink term $\phi$ accounts for the breakdown of chemicals in both the liquid and solid phases, expressed as:

$$\phi=\mu_L\theta C+\mu_S\rho s \tag{9}$$

where $\mu_L$and $\mu_S$ are the first-order degradation rate constants in the liquid and solid phases [$T^{-1}$], respectively. These rates can be derived from the half-life value $t_{1/2}$ [$T^{-1}$] as $\mu$=ln(2)/$t_{1/2}$. For non-reactive solutes like bromide, adsorption and degradation processes are not considered (i.e., $K_d$=0, and $\mu$=0). For pesticides, both adsorption/desorption and degradation processes are considered.

### 2.2.2 Initial and boundary condition settings

Each soil profile was divided into nine layers: five for the top 2.5 m of the shallow vadose zone and four additional layers extending to 70 m to represent the deep unsaturated zone. The shallow layers were determined based on soil core sample measurements (shown in Table S1), while the deeper layers were informed by tTEM sediment texture data (shown in Table S2 and Fig. S1).

In the shallow zone (0-2.5 m) (Fig. 2a), the 250 cm soil profile was divided into five distinct modeling layers: 0–46 cm, 47–76 cm, 77–122 cm, 123–182 cm, and 183–250 cm. These layers were created by grouping the original soil texture data and aligning each layer with corresponding sensors installed at depths of 0.2, 0.6, 1, 1.75, and 2.5 m (Table S1). The spatial discretization resolution was 1 cm throughout the soil profile. Initial soil pressure heads were set based on field measurements of soil water contents at 0.2, 0.6, 1.0, and 2.5 m (Fig. S2), while the initial solute concentrations (bromide and pesticides) were based on pore water data. For water flow, the upper boundary condition was set to an atmospheric flux (considering precipitation, evaporation, and flooding, Fig. S3), while the lower boundary condition was set to free drainage. Solute transport had a Cauchy boundary condition at the surface, adjusting for bromide concentrations during irrigation, with a zero-concentration gradient (Neumann boundary) at the lower boundary (Text S2). The soil hydraulic parameters ($\theta_s$, $\alpha$, $n$, $K_s$) and reactive solute transport parameters ($\lambda$, $K_d$ , $\mu_L$and $\mu_S$) in the shallow (2.5 m) vadose zone were optimized (discussed later in Sections 2.3).

For the deep unsaturated zone (2.5-70 m) (Fig. 2b), four additional layers (Layers 6-9) were incorporated to reflect the coarse and fine sediment texture classifications from the tTEM data. Since texture and sediment hydraulic properties (e.g., $K_s$) cannot



11

yet be reliably estimated from tTEM data (Perzan et al., 2023), we explored different permutations of seven fine-textured materials (clay to sandy clay), and five coarse-textured (loam to sand) materials as stated in Table S2. Layers 7 (5-20 m) and 9 (35-70 m), which were classified as consisting of coarse materials in the tTEM data were assigned 5 soil textures, while layers 6 (2.5-5 m) and 8 (20-35 m), which included both fine and coarse materials in the tTEM classification were assigned 12 textures (clay to sandy clay) from the United States Department of Agriculture (USDA) soil texture triangle (Table S2). Different combinations of USDA textures for the fine and coarse soil layers resulted in 3600 soil texture combinations (12*5*12*5) for each soil profile. These soil profiles were generated to evaluate the role of soil texture on pesticide transport. The spatial discretization of the deep vadose zone is 50 cm. The bottom boundary conditions of the deep vadose zone model are a constant pressure head for water flow (i.e., pressure head equals zero at 70 m) and a zero concentration gradient for pesticide transport (Text S2). For simplicity, the adsorption and degradation coefficients, along with initial pesticide concentrations in the deep unsaturated zone (2.5-70 m), were set to 0. The initial pressure heads in the deep vadose zone (2.5 to 70 m) were defined as a constant pressure gradient, starting from a specific value at a depth of 2.5 m and gradually increasing to zero at the groundwater table (Fig. S2). The transport parameters (dispersivities) were fixed as 700 cm (i.e., 1/10th of the total travel distance (Gelhar et al., 1992). Thus, only the effects of soil hydraulic parameters ($\theta_s$, $\alpha$, $n$, $K_s$) were included in the deep unsaturated zone model runs.

The simulation period was 104 days, from 0:00 on Dec. 17, 2020, to 24:00 on Mar. 31, 2021, which included pre-flooding (before Feb. 16), flooding (Feb. 16~Feb. 24), and post-flooding (after Feb. 24) periods. The temporal discretization resolution was variable, with a minimum time step of 0.01 minutes. After each run, the maximum transport depths (MTDs) (i.e., the depth where the pesticide concentration was zero) during the Ag-MAR period (Feb. 16 to Feb. 24, 2021) were recorded for both a



12

business-as-usual scenario (Rainfall scenario - no Ag-MAR but rainfall only) and an Ag-MAR scenario (MTD_Rainfall and MTD_Ag-MAR). The relative difference in MTDs for a specific pesticide between Rainfall and Ag-MAR scenarios (i.e., RMTD) was calculated as (MTD_Ag-MAR – MTD_Rainfall)/MTD_Rainfall.

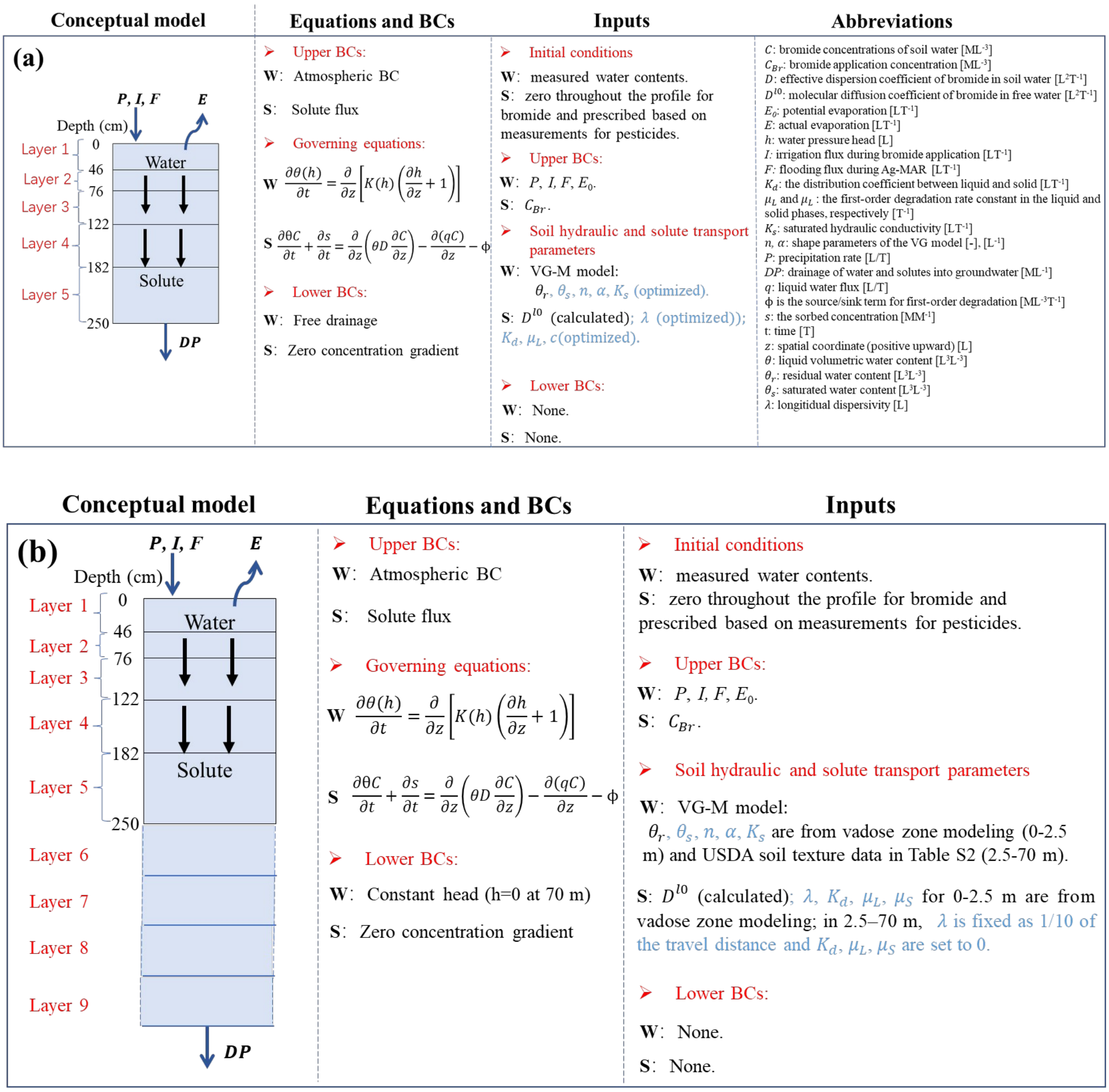


$$W \quad \frac{\partial\theta(h)}{\partial t} = \frac{\partial}{\partial z}\left[K(h)\left(\frac{\partial h}{\partial z}+1\right)\right]$$

$$S \quad \frac{\partial\theta C}{\partial t} + \frac{\partial s}{\partial t} = \frac{\partial}{\partial z}\left(\theta D\frac{\partial C}{\partial z}\right) - \frac{\partial(qC)}{\partial z} - \phi$$

Figure 2. HYDRUS-1D model setup for the vadose zones (a) 0-2.5 m and (b) 0-70 m deep. Note that “W” and “S” represent water flow and solute transport, respectively.

## 2.3 Parameter optimization and Bayesian inference

In this study, we adopted a two-step optimization for the shallow 2.5 m vadose zone. In the first step, we calibrated soil hydraulic parameters and dispersivities using measured bromide breakthrough curves (BTCs) since bromide is not influenced by adsorption, desorption, or degradation. The residual water content ($\theta_r$) was not optimized. Instead, the default values for corresponding soil textures were initially adopted and then manually adjusted to improve the model fit, as done in many other studies (Schaap and Bouten, 1996; Vereecken et al., 2010; Wosten and van Genuchten, 1988; Zhou et al., 2022). Therefore, five parameters ($\theta_s$, $\alpha$, $n$, $K_s$, and $\lambda$) were optimized for each layer.

The Gradient-Based Comprehensive Learning Particle Swarm Optimization (G-CLPSO) method (Brunetti et al., 2022) was used to inversely estimate soil hydraulic parameters and dispersivities ($\theta_s$, $\alpha$, $n$, $K_s$, and $\lambda$) for five different soil horizons (i.e., a total of 25 calibrated parameters) at each of the three soil profiles (P1, P2, P3). Measured surface pressure heads, volumetric water contents, and bromide concentrations at different depths were used in the calibration process.

G-CLPSO combines the exploration and exploitation capabilities of the Comprehensive Learning Particle Swarm Optimization (Liang et al., 2006) and Marquardt-Levenberg search strategy, respectively. The sum of squared residuals between observed and simulated values is the objective function. The swarm population and the learning parameter were set to 20 and 1.4995, respectively. A random individual was selected every three iterations and used as a starting point for the Marquardt-Levenberg search. The algorithm was considered converged if all particles' best positions and the global best position recorded for the entire swarm simultaneously exhibited negligible improvements in the last five consecutive iterations. An improvement was considered negligible if the relative change in the objective function between two consecutive iterations was below a user-defined tolerance value of 0.1%. The 95% confidence intervals were calculated for each parameter to assess the uncertainty. Optimized parameters and their uncertainty are summarized in Table S5.



14

In the second step, soil hydraulic parameters and dispersivities ($\theta_s$, $\alpha$, $n$, $K_s$, and $\lambda$) were set to their previously calculated global optima (Table S5). Pesticide BTCs at different depths were combined with the Bayesian inference to inversely estimate adsorption and reaction parameters and assess their uncertainty. In particular, the distribution coefficient $K_d$ and the first-order degradation coefficients in the liquid and solid phases, $\mu_L$and $\mu_S$, for five different soil horizons were calibrated for a total of 15 parameters.

Uniform priors were set for all parameters, while measurement errors were assumed uncorrelated and normally distributed with a constant variance, $\sigma^2$. Considering the complexity of the field-scale experiment, which increased uncertainty, pesticide concentration observations at different depths were normalized by their maxima, and $\sigma$ was set to 0.2. The G-CLPSO method was first used to identify a high-likelihood region in the parameters' space, from which multiple Markov chains were initialized (Brunetti et al., 2023). In particular, a Markov Chain Monte Carlo (MCMC) method based on the Affine Invariant Ensemble Sampler (Goodman and Weare, 2010) was used to approximate the parameters' posterior distribution. As Brunetti et al. (2023) suggested, a total of 30 chains evolved for 10,000 steps to achieve stationary distributions. The Python package *emcee* was used to carry out the Bayesian analysis. Optimized parameters and their uncertainty are summarized in Tables S6-S9.

### 2.4 Model Sensitivity, Information Content of Observations, and Parameter Interactions

The estimated posterior distributions of parameters from Section 2.3 and a parameter correlation analysis using the Jacobian approximation of the Hessian matrices around the optima (Šimůnek and Hopmans, 2002) were combined to detect and analyze parameters' interaction, as shown in Figs. S10-S24. The estimated posterior distributions of parameters provide a statistical basis to clarify how observations inform



15

model parameters and identify which parameters are most sensitive for the calibration process. The statistic metric that summarizes these effects is the Kullback-Leibler divergence $D_{KL}$ between the prior $\pi(x)$ and the posterior $p(x)$ for each parameter:

$$D_{KL}(\pi(x) \vee ¿ p(x)) = \int_x \pi(x) \log \frac{\pi(x)}{p(x)} dx$$

$D_{KL}$ is positively correlated with the information content of the observations. Parameters characterized by relatively high $D_{KL}$ are informed by the data and thus influence the model fitting (i.e., sensitive factors). Parameter interactions are analyzed using correlation matrices and marginal posterior distributions for water flow, tracer transport, and pesticide reactive transport. The former is based on the final covariance matrices obtained by the G-CLPSO algorithm around the global optima, while the latter is a direct outcome of the Bayesian inference.

# 3 Results

## 3.1 Model parameters and performance

The estimated soil hydraulic and pesticide transport, adsorption, and reaction parameters and their uncertainty for the upper 2.5 m of the unsaturated zone are summarized in Tables S5-S9. With a few exceptions, the optimized soil hydraulic parameters for the observed soil textures were within the typical ranges reported in other studies (Text S4). Although all three Ag-MAR sites were classified as Traver fine sandy loam, P1 and P3 had a distinct cemented duripan at a depth of 77-122 cm (Bachand et al., 2014), resulting in lower saturated hydraulic conductivities ($K_s$) at these depths (approximately 0.005-0.01 cm/min). Overall, $K_s$ values were highest at P2, the sandiest profile (84% sand), lowest at P1 (41% sand), and intermediate at P3 (61% sand). The estimated adsorption and degradation coefficients for the pesticides generally followed the opposite trend, being highest at P1 and lowest at P2, consistent



16

with the total organic matter content (Table S1). Additionally, *Chlorantraniliprole* and *Methoxyfenozide* exhibited higher adsorption, but lower degradation rates compared to *Imidacloprid* and *Thiamethoxam* (Tables S6-S9), indicating they were less mobile and more persistent in the environment.

The simulated versus observed pesticide concentrations for *Imidacloprid*, *Thiamethoxam*, *Chlorantraniliprole*, and *Methoxyfenozide* across the three profiles (P1, P2, and P3) showed the model's ability to capture overall transport trends (Fig. 3 and Figs. S7-S9; Table 1). For *Imidacloprid*, the model fit well at shallow depths, with larger discrepancies at deeper levels, particularly in Profile 2 (Fig. 3). *Thiamethoxam* showed good agreement at shallow depths, but deeper levels, especially in Profile 3, reflected underestimations (Fig. S7). *Chlorantraniliprole* showed satisfactory simulation accuracy across most profiles and depths, but significant underestimations occur at 250 cm in Profile 2 (Fog. S6). *Methoxyfenozide* was well captured at shallow depths, but deeper levels, particularly in Profile 2, show underestimation (Fig. S9). Overall, the model reasonably approximated pesticide transport in the shallow vadose zone but required refinements for the deeper unsaturated zones to better account for potential preferential flow and kinetic adsorption (i.e., physical and chemical nonequilibrium) since rapid water flow during intensive flooding makes it more challenging to reach adsorption equilibrium (Dusek et al., 2015).

Table 1. Mean root mean square deviation (RMSE) for simulating surface ponding levels, soil water contents, concentrations of bromide and four pesticides (*Imidacloprid*, *Thiamethoxam*, *Chlorantraniliprole*, *Methoxyfenozide*) in the shallow vadose zone (0-2.5 m) of the three soil profiles (P1, P2, P3).

| Profile | P1 | P2 | P3 |
|---|---|---|---|
| Surface ponding level (cm) | 1.61 | 2.36 | 2.43 |
| Water content ($cm^3/cm^3$) | 0.03 | 0.05 | 0.03 |
| Bromide (ppm) | 45.29 | 22.68 | 36.29 |
| *Imidacloprid* (ppb) | 0.12 | 0.15 | 0.21 |



17

| | | | |
|---|---|---|---|
| *Thiamethoxam* (ppb) | 1.20 | 0.68 | 2.15 |
| *Chlorantraniliprole* (ppb) | 1.54 | 2.99 | 0.27 |
| *Methoxyfenozide* (ppb) | 0.21 | 0.20 | 0.09 |

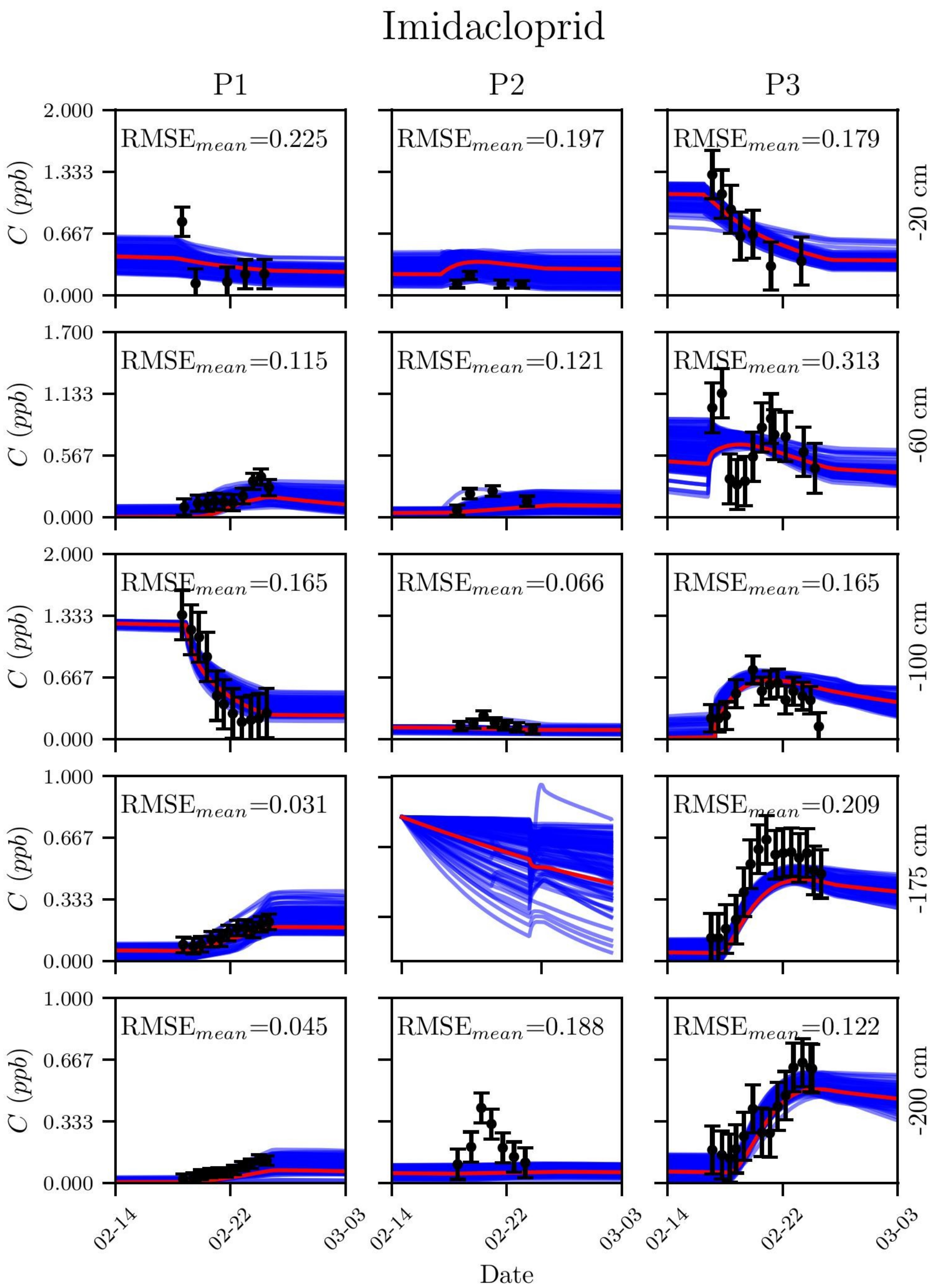


Figure 3. Observed (black dots with vertical error bars) and simulated (black lines) *Imidacloprid* concentrations at different depths (20, 60, 100, 175, and 250 cm; top to bottom) for the three soil profiles (P1, P2, P3; left to right). The blue shaded

area is obtained by randomly sampling 100 solutions from the posterior parameter distributions obtained by Bayesian Inference (Tables S6-S9). The mean root mean square deviation (RMSEmean) for simulations using the mean parameters values (red line) is also reported.

### 3.2 Parameters' sensitivity and interactions and observations information content

The Kullback-Leibler divergence ($D_{KL}$) was used to illustrate the sensitivity of different parameters in predicting the behavior of four pesticides in the upper 2.5 m of the unsaturated zone across the three soil profiles (Fig. 4). Parameters with higher $D_{KL}$ values are more sensitive, indicating that their changes more significantly impact the model's accuracy (Schübl et al., 2022). In particular, degradation coefficients ($\mu_L$and $\mu_S$) were particularly sensitive for *Imidacloprid* at P2 and *Thiamethoxam* at P1, respectively. This is also confirmed by the joint marginal posterior (Figs. S16 and S12), which was leptokurtic for these parameters. Conversely, adsorption coefficients were more relevant for *Thiamethoxam* at P3 and *Chlorantraniliprole* at P1, respectively. Interestingly, *Methoxyfenozide* exhibited consistently high $D_{KL}$ for most parameters at profile P2, which were reflected in the right skewed joint posterior (Fig. S19). This type of posterior distribution indicates structural model inadequacy, which forces the calibrated parameters towards physically unrealistic values. From a Bayesian point of view, this implies that only a few parameter sets are likely to have produced data generating processes. However, this inadequacy is here mainly attributed to measurement inaccuracies, since results for *Methoxyfenozide* at other soil profiles are satisfactory.



19

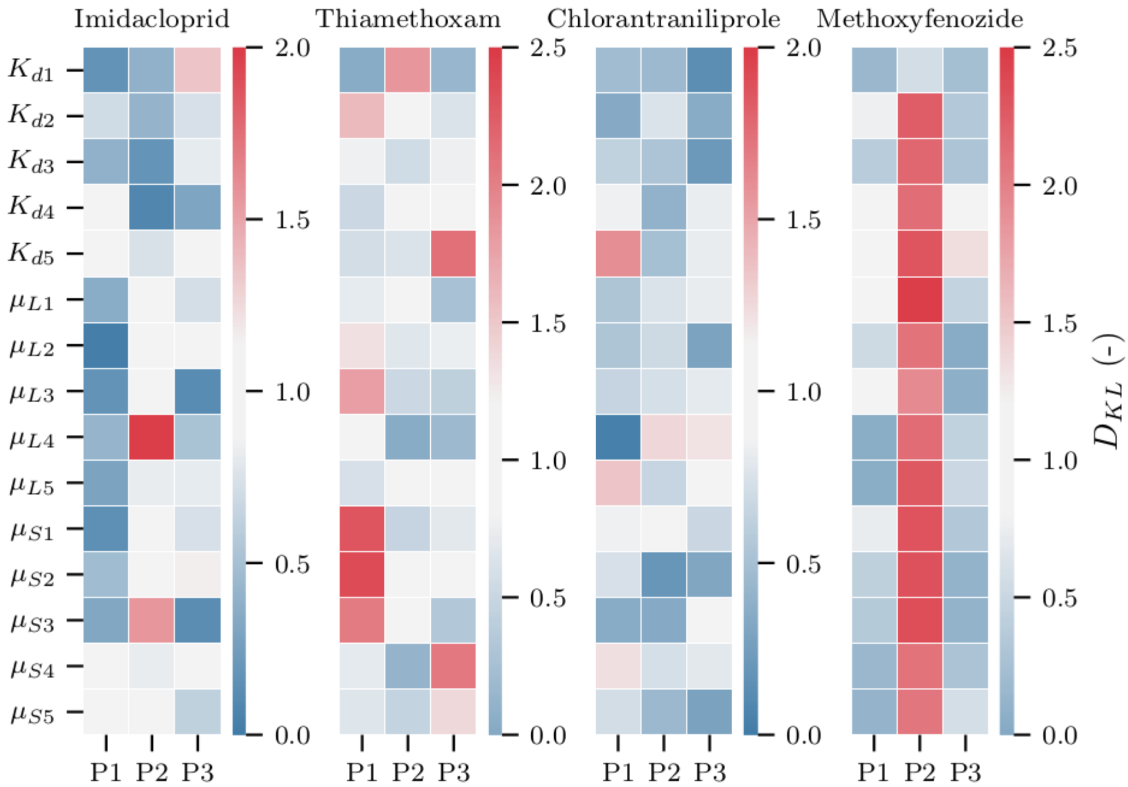


Figure 4. Kullback-Leibler divergence $D_{KL}$ of degradations in the liquid ($\mu_L$) and solid ($\mu_s$) phases and adsorption ($K_d$) in different layers (1,2,3,4,5) of the three soil profiles (P1, P2, P3) for *Imidacloprid*, *Thiamethoxam*, *Chlorantraniliprole*, and *Methoxyfenozide*.

### 3.3 Pesticide leaching dynamics

Pesticide transport responded strongly to the infiltrating floodwater applied for eight continuous days in February 2021 at the site (Fig. 3 and Figs. S7-S9). Water samples taken at three locations from five depths in the upper 2.5 m of the unsaturated zone showed measurable concentrations of *Imadocloprid*, *Methoxyfenozide*, *Thiamethoxam*, and *Chlorantraniliprole*. Pesticides were applied 7 (*Chlorantraniliprole*, *Thiamethoxam*), 8.5 (*Imadocloprid*), and 29 (*Methoxyfenozide* ) months before the recharge experiment (Table S2 in Zhou et al., 2024), likely explaining the one order of magnitude difference in concentrations between *Chlorantraniliprole* or *Thiamethoxam* and the other two pesticides. Maximum concentrations of the four pesticides ranged between 1.3 – 13.3 ppb in Profile 1 (P1), 0.4 – 13.2 ppb in Profile 2 (P2), and 1.3 – 22.5 ppb in Profile 3 (P3).

Shallow soil layers (0-122 cm) showed the most significant decrease in pesticide concentrations, likely due to strong leaching from these layers, except for *Methoxyfenozide*, whose concentrations increased. Increasing *Methoxyfenozide* concentrations suggest chemical nonequilibrium transport and recharge-facilitated release of *Methoxyfenozide* into the pore water. Pesticide concentrations in larger depths (122-250 cm) varied between profiles: rising (mostly at P1), falling (mostly at P2), or initially rising then falling (mostly at P2 and P3). These patterns indicate different arrival rates of peak pesticide concentrations during flooding: slower at P1, faster at P2, and medium at P3, suggesting that pesticide transport is strongly controlled by sediment texture, as the P2 profile, with the highest sand fraction (84%), showed the fastest leaching among all profiles.

### 3.4 Water and pesticide mass balances and flooding water travel times

Water mass balance (Table 2), pesticide mass balance (Table 3) and flooding water travel times (Table 4) were calculated for the upper 2.5 m of the unsaturated zone. The largest groundwater recharge (93.6%; Table 2) was observed at P2, the smallest (87.3%) at P1, while P3 (87.6%) was between the two but closer to P1. The water mass balance between P2 and the other two profiles varied by up to 7%.

The highest leaching efficiency of *Chlorantraniliprole* and *Methoxyfenozide* (3.8-6.2%) was reached at P2. The highest leaching efficiency of *Imidacloprid* (1.3-20.4%) was observed at P3, while the lowest (0.1-12.7%) was at P1 (Table 3). This finding was supported by the fact that the adsorption and degradation coefficients were largest at P1, followed by P3, while the lowest were at P2, as discussed in Section 3.1.

As expected, the P2 profile with the highest sand content produced the shortest travel times and highest flow velocities due to its greater permeability, followed by P3, while P1 had the lowest. However, at some depths, P3 showed shorter travel times and higher velocities, likely due to localized coarse textures that enhanced water movement despite its lower overall sand content. Accordingly, bromide travel times or transport velocities between the three profiles differed by up to 80.6%, ranging between 0.35-6.97 days or between 11.11-61.22 cm/day in the 2.5 m of the near-surface unsaturated zone (Table 4).

Table 2. Water mass balance components for three soil profiles.

| Term | P1 | | P2 | | P3 | |
|---|---|---|---|---|---|---|
| | cm | % | cm | % | cm | % |
| P+I | 128.4 | | 128.4 | | 128.4 | |
| E | 13.3 | 10.3 | 9.6 | 7.5 | 12.2 | 9.5 |
| D | 111.3 | 86.6 | 116.8 | 91.0 | 112.6 | 87.7 |
| $\Delta S_{RZ}$ | 6.9 | 5.4 | 2.7 | 2.1 | 7.6 | 5.9 |
| $\Delta S_{LZ}$ | 0.8 | 0.6 | 3.3 | 2.6 | -0.1 | 0.0 |
| GR | 112.1 | 87.3 | 120.1 | 93.6 | 112.5 | 87.6 |

P: precipitation, F: flooding and irrigation, E: evaporation, D: drainage, $\Delta S$: storage change in the root zone 0~100 cm ($\Delta S_{RZ}$) and deep vadose zone 100-250 cm ($\Delta S_{LZ}$), GR: groundwater recharge including D and $\Delta S_{LZ}$ because water flow is considered to be one-dimensional and thus deep drainage below the root zone will eventually recharge groundwater with a delay (de Vries and Simmers, 2002).



22

Table 3. Solute mass balance components for four pesticides at three soil profiles.

| | | P1 | | | P2 | | | P3 | | |
|---|---|---|---|---|---|---|---|---|---|---|
| Pesticide | Term | ppb●cm | Mean (%) | Range (%) | ppb●cm | Mean (%) | Range (%) | ppb●cm | Mean (%) | Range (%) |
| Imidacloprid | $S_{p,init}$ | 664.0 | | | 519.1 | | | 219.1 | | |
| | $L_p$ | -3.9 | 0.6 | 0-13.4 | -6.5 | 1.3 | 0.2-15.4 | -44.7 | 20.4 | 3.5-52.5 |
| | $D_p$ | -432.0 | 65.1 | 10-85.9 | -198.6 | 38.3 | 2.6-77.2 | -100.3 | 45.8 | 3.4-79 |
| | $S_{p,fin}$ | 227.1 | 34.2 | 13.6-76.6 | 314.1 | 60.5 | 22.7-82 | 74.2 | 33.9 | 17.5-44.1 |
| | $\Delta S_{p,.}$ | -321.9 | | | -119.8 | | | -147.5 | | |
| | $\Delta S_{p,.}$ | -115.0 | | | -85.3 | | | 2.6 | | |
| Thiamethoxam | $S_{p,init}$ | 2441.9 | | | 2842.4 | | | 8898.0 | | |
| | $L_p$ | -309.9 | 12.7 | 8.4-20.5 | -153.5 | 5.4 | 1.9-20.5 | -117.4 | 1.3 | 0.2-15.7 |
| | $D_p$ | -431.2 | 17.7 | 1.1-29.6 | -2555.5 | 89.9 | 73.1-97.8 | -7437.5 | 83.6 | 48.1-94.2 |
| | $S_{p,fin}$ | 1709.4 | 70.0 | 62.2-78.9 | 133.3 | 4.7 | 0.7-6.2 | 1300.4 | 14.6 | 4.8-36.1 |
| | $\Delta S_{p,.}$ | -654.7 | | | -487.2 | | | -2518.6 | | |
| | $\Delta S_{p,.}$ | -77.9 | | | -2222.0 | | | -5078.9 | | |
| Chlorantraniliprole | $S_{p,init}$ | 6519.8 | | | 1754.5 | | | 1996.7 | | |
| | $L_p$ | -7.5 | 0.1 | 0-2.1 | -67.2 | 3.8 | 3.8-31.2 | -56.3 | 2.8 | 0.2-12.1 |
| | $D_p$ | -1253.0 | 19.2 | 3.8-21.9 | -456.5 | 26.0 | 0.2-26 | -293.3 | 14.7 | 3.4-47.2 |
| | $S_{p,fin}$ | 5259.8 | 80.7 | 78.1-94.2 | 1231.2 | 70.2 | 68.4-70.2 | 1647.2 | 82.5 | 52.4-84.5 |
| | $\Delta S_{p,.}$ | -1097.6 | | | -694.6 | | | -399.6 | | |
| | $\Delta S_{p,.}$ | -162.3 | | | 171.4 | | | 50.1 | | |
| Methoxyfenozide | $S_{p,init}$ | 699.1 | | | 243.0 | | | 705.2 | | |



23

| | | | | | | | | | |
|---|---|---|---|---|---|---|---|---|---|
| $L_p$ | -2.6 | 0.4 | 0-16.6 | -15.0 | 6.2 | 6.2-33.1 | -8.9 | 1.3 | 0.2-9.4 |
| $D_p$ | -331.1 | 47.4 | 11.5-60.4 | -10.4 | 4.3 | 0-15.3 | -184.2 | 26.1 | 3.6-45.1 |
| $S_{p,fin}$ | 365.1 | 52.2 | 39.3-72 | 217.6 | 89.6 | 66.9-89.6 | 512.0 | 72.6 | 54.5-87 |
| $\Delta S_{p,}$ | -73.7 | | | -28.9 | | | -192.1 | | |
| $\Delta S_{p,}$ | -5.0 | | | 3.5 | | | -1.2 | | |

Note that $S_{init}$ and $S_{final}$ are the initial and final pesticide storages in the soil profile, respectively, $L_p$ is the pesticide leaching through drainage, $D_p$ is the degradation due to chemical or biological reactions, and $\Delta S_p$ is a pesticide storage change in the root zone 0~100 cm ($\Delta S_{p,RZ}$) and deep vadose zone 100-250 cm $\Delta S_{p,LZ}$

..



24

Table 4. Travel times and average velocities of bromide (calculated by the peak displacement method) from the soil surface to different soil depths at three soil profiles.

| Term | Depth (cm) | P1 | P2 | P3 |
|---|---|---|---|---|
| Travel time (day) | 20 | 1.80 | 1.10 | 0.35 |
| | 60 | 2.64 | 1.64 | 0.98 |
| | 100 | 3.72 | 2.26 | 2.15 |
| | 175 | 5.68 | 4.01 | 3.90 |
| | 250 | 6.97 | 4.55 | 4.90 |
| Flow velocity (cm/day) | 20 | 11.11 | 18.18 | 57.14 |
| | 60 | 22.73 | 36.59 | 61.22 |
| | 100 | 26.88 | 44.25 | 46.51 |
| | 175 | 30.81 | 43.64 | 44.87 |
| | 250 | 35.87 | 54.95 | 51.02 |

### 3.5 The maximum transport depth (MTD) of pesticides during the Ag-MAR period

The 2.5 m model domains of the calibrated models were extended to 70 m using the coarse and fine texture sediment classifications obtained using the towed transient electromagnetic (tTEM) data (Goebel and Knight, 2021) to estimate the maximum transport depths of the four pesticides in the deep unsaturated zone. Fig. 5 compares the pesticides' maximum transport depths (MTDs) for the tTEM-mapped fine- and coarse-textured layers shown in Table S2 for the Ag-MAR and Rainfall scenarios. MTD is defined in this study as the soil profile depth where the concentration of a given pesticide falls to zero. It represents the maximum vertical extent to which a pesticide is transported in the unsaturated zone.

Fig. 6 and Table 5 show the mean values and standard deviations of MTDs. In Profile P1, the mean MTD values under the Rainfall scenario range between 7.64 m and 8.15 m, with standard deviations between 1.50 m and 1.59 m. Under the Ag-MAR scenario, pesticides traveled much deeper, with mean MTD values from 16.66 m to 17.02 m and standard deviations between 3.13 m and 3.17 m. In Profile P2, the Rainfall scenario resulted in mean MTD values between 7.69 m and 8.15 m, with standard deviations from 1.33 m to 1.55 m. In contrast, the Ag-MAR scenario showed deeper transport, with mean MTDs ranging from 17.86 m to 18.17 m and standard deviations around 3.44 m. In Profile P3, the Rainfall scenario showed mean MTD values between 5.73 m and 8.15 m, with standard deviations between 1.57 m and 1.72 m. Under Ag-MAR, mean MTD values increased significantly, ranging from 15.85 m to 17.48 m, with standard deviations from 3.05 m to 3.09 m. The results indicate that the application of 1.2 $m^3/m^2$ of water in the Ag-MAR scenario increased the MTDs for all pesticides in all profiles, as indicated by a consistent downward shift of MTDs compared to the Rainfall scenario. The Ag-MAR scenario shows greater variability (higher standard deviations), indicating that Ag-MAR practices resulted in more variable pesticide transport depths. Overall, Profile P2 generally showed the deepest MTDs across both scenarios, followed by P3 and P1. *Thiamethoxam* generally showed the largest MTDs, while *Methoxyfenozide* showed the smallest MTDs in the unsaturated zone of all soil profiles in response to the Ag-MAR or Rainfall scenarios (Fig. 6 and Table 5).

Fig. 7 and Table 5 show the relative differences in MTDs of pesticides between the Ag-MAR and Rainfall scenarios (i.e., RMTDs). The RMTD is expressed as a percentage increase in the maximum transport depth under Ag-MAR relative to the Rainfall scenario. In P1, the RMTD values ranged from 116.6% ± 42.9% for *Thiamethoxam* to 123.6% ± 47.9% for *Methoxyfenozide*. In P2, the RMTD values ranged from 130.3% ± 39.4% for *Thiamethoxam* to 138.9% ± 60.6% for *Methoxyfenozide*. In P3, the RMTD values ranged from 111.5% ± 52.1% for *Thiamethoxam* to 159.4% ± 53.5% for *Methoxyfenozide*. Overall, RMTDs were larger at P2 than at P1 and P3. *Thiamethoxam* generally showed the lowest RMTDs, while *Methoxyfenozide* showed the largest RMTDs in the unsaturated zone of all profiles in response to the Ag-MAR or Rainfall scenarios.

Interestingly, under the Rainfall scenario, the impact of the deep vadose zone soil textures on pesticide transport was minimal, with similar MTD values observed across various soil textures (Figs. 5a-5f). However, a subtle pattern emerged, indicating that finer-textured soils in Layers 6 and 7 (2.5-20 meters) resulted in slightly deeper MTDs (Figs. 5a-5f). This is because finer soils have a higher unsaturated hydraulic conductivity than coarser soils during drier conditions (in the Rainfall scenario), allowing water to flow more consistently downward. As a result, pesticides were transported deeper in fine soils. In contrast, a clear and consistent trend was observed under the Ag-MAR scenario, where coarser-textured soils in Layers 6 and 7 (2.5-20 meters) led to significantly deeper MTDs (Figs. 5a-5f). During wetter conditions in the Ag-MAR scenario, there were stronger hydraulic gradients, pushing larger volumes of water with dissolved pesticides further into the deep vadose zone, particularly through coarser soils that allowed for faster water movement due to their larger pores and higher saturated hydraulic conductivities.

The occurrence of a coarser textured layer at the depths of 2.5-5 m (Layer 6) or 5-20 m (Layer 7) in Profiles 1 and 3 significantly impacted MTDs under Ag-MAR, while the finer or coarser-textured layers below (Layer 8: 20-35 m and Layer 9: 35-70 m) had only a minor effect on pesticide transport. When the soil textures at Layers 6 or 7 were not loamy sand or sand, MTDs under Ag-MAR can be controlled within the first 20 m of the unsaturated zone for any other soil texture considered (Fig. 5a-5f).

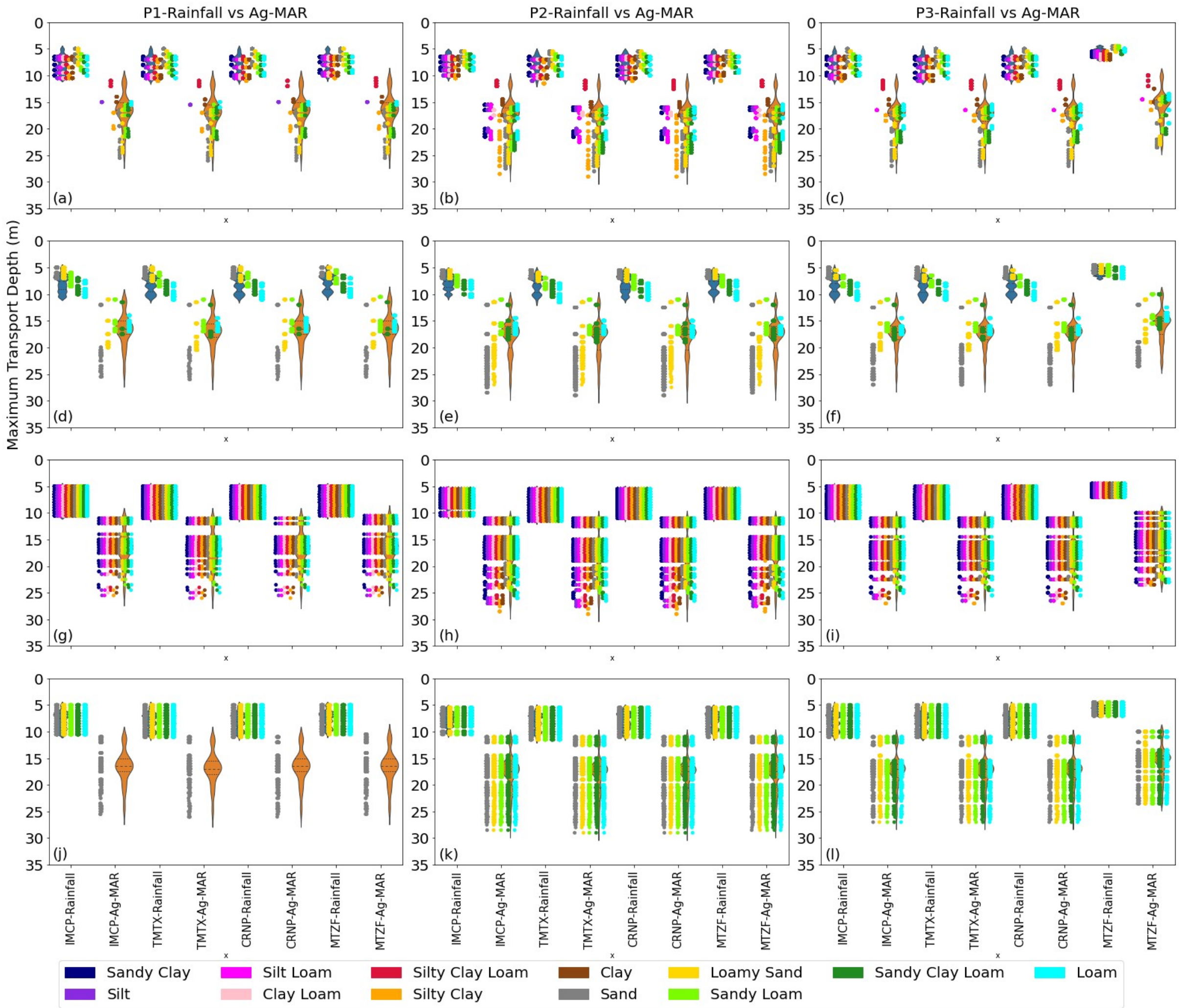


Figure 5. Violin plots of the maximum transport depths (MTDs) of the four pesticides, including *Imidacloprid* (IMCP), *Thiamethoxam* (TMTX), *Chlorantraniliprole* (CRNP), and *Methoxyfenozide* (MTFZ) during the Ag-MAR period (Feb. 16 to Feb. 24, 2021) in response to the Rainfall and Ag-MAR scenarios and different soil texture permutations (Table S2) reflecting fine and coarse textured materials in the deep unsaturated zone. MTDs are shown for the fine/coarse-textured Layer 6 (2.5-5 m) (plots a-c), coarse-textured Layer 7 (5-20 m) (plots d-f), the fine/coarse-textured Layer 8 (20-35 m) (g-i), and the coarser-textured Layer 9 (35-70 m) (j-l) for the three soil profiles (P1, P2, P3).

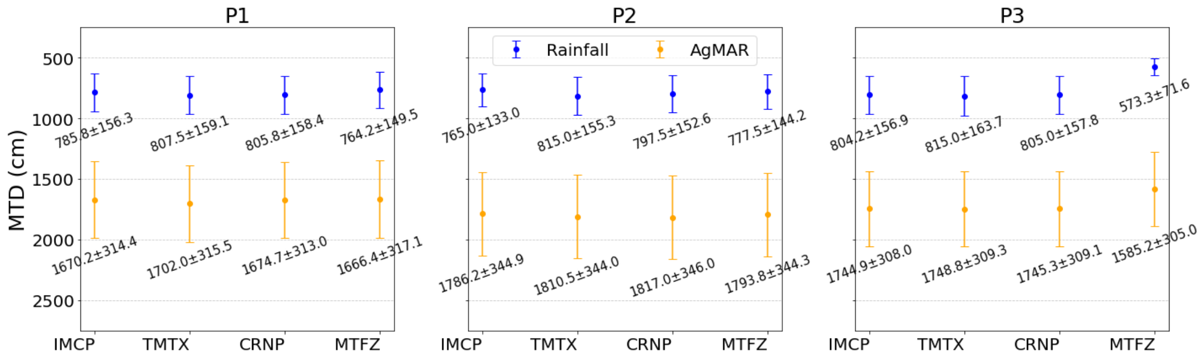


Figure 6. Comparison of mean values and standard deviations of maximum transport depths (MTDs) for the four pesticides, including *Imidacloprid* (IMCP), *Thiamethoxam* (TMTX), *Chlorantraniliprole* (CRNP), and *Methoxyfenozide* (MTFZ) during the Ag-MAR period (Feb. 16 to Feb. 24, 2021) in response to the Rainfall and Ag-MAR scenarios. The markers represent the mean values, and error bars indicate standard deviations.

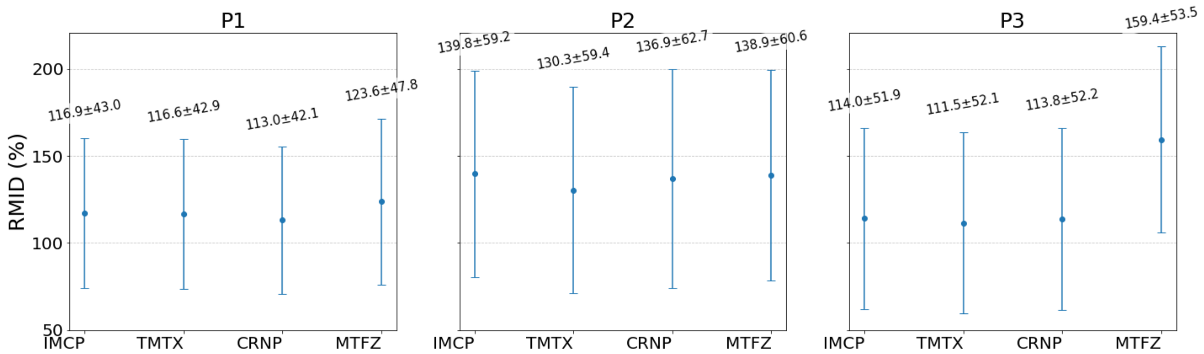


Figure 7. Comparison of the mean values and standard deviations of relative differences in the maximum transport depths (RMTD) for the four pesticides, including *Imidacloprid* (IMCP), *Thiamethoxam* (TMTX), *Chlorantraniliprole* (CRNP), and *Methoxyfenozide* (MTFZ) during the Ag-MAR period (Feb. 16 to Feb. 24, 2021) between the Rainfall and Ag-MAR scenarios. The markers represent the mean values, and error bars indicate standard deviations.

Table 5. Impact of Ag-MAR on water flow and pesticide transport across the three soil profiles (P1, P2, P3).

| Indicators | | P1 | P2 | P3 |
|---|---|---|---|---|
| Water flow | Sand content | 41% | 84% | 61% |
| | Capillary barrier at 5-20 m | Yes | No | Yes |
| | Recharge efficiency (%) | 87.3 | 93.6 | 87.6 |
| | Flow velocity (cm/day) | 11.11-35.87 | 18.18-54.95 | 44.87-61.22 |
| *Imidacloprid* | Leaching efficiency (%) | 0-13.4 | 0.2-15.4 | 3.5-52.5 |
| | MTD_Rainfall (m) | 7.86±1.56 | 7.65±1.33 | 8.04±1.57 |
| | MTD_Ag-MAR (m) | 16.70±3.14 | 17.86±3.45 | 17.45±3.08 |

| | | | | |
|---|---|---|---|---|
| | RMID (%) | 116.9±43.0 | 139.8±59.2 | 114.0±51.9 |
| *Thiamethoxam* | Leaching efficiency (%) | 8.4-20.5 | 1.9-20.5 | 0.2-15.7 |
| | MTD_Rainfall (m) | 8.08±1.59 | 8.15±1.55 | 8.15±1.64 |
| | MTD_Ag-MAR (m) | 17.02±3.16 | 18.11±3.44 | 17.49±3.09 |
| | RMID (%) | 116.6±42.9 | 130.3±59.4 | 111.5±52.1 |
| *Chlorantraniliprole* | Leaching efficiency (%) | 0-2.1 | 3.8-31.2 | 0.2-12.1 |
| | MTD_Rainfall (m) | 8.06±1.58 | 7.98±1.53 | 8.05±1.58 |
| | MTD_Ag-MAR (m) | 16.75±3.13 | 18.17±3.46 | 17.45±3.09 |
| | RMID (%) | 113.0±42.1 | 136.9±62.7 | 113.8±52.2 |
| *Methoxyfenozide* | Leaching efficiency (%) | 0-16.6 | 6.2-33.1 | 0.2-9.4 |
| | MTD_Rainfall (m) | 7.64±1.50 | 7.78±1.44 | 5.73±0.72 |
| | MTD_Ag-MAR (m) | 16.67±3.17 | 17.94±3.44 | 15.85±3.05 |
| | RMID (%) | 123.6±47.8 | 138.9±60.6 | 159.4±53.5 |

Note that MTD is the maximum transport depth (i.e., the depth where the pesticide concentration is zero) from Feb. 16 to Feb. 24, 2021 (i.e., Ag-MAR time period) for Rainfall and Ag-MAR scenarios (MTD_Rainfall and MTD_Ag-MAR).

# 4 Discussion

## 4.1 Comparison of findings with Zhou et al. (2024)

Both studies evaluated model performance (Section 3.1), with both achieving good results for surface water levels and soil moisture but facing challenges in predicting pesticide concentrations at deeper soil depths of the upper 2.5 m unsaturated zone. In this study, significant deviations between the observed and simulated pesticide residue concentrations occurred in P2 for *Imidacloprid* and *Methoxyfenozide*. Similarly, Zhou et al. (2024) found that preferential flow paths in deeper layers made it difficult for models to accurately predict pesticide movement. Dual-porosity models (DPM) helped improve surface water and bromide predictions in Zhou et al. (2024), but they still struggled with pesticide dynamics, highlighting the need for better models to account for complex flow paths and slow chemical reactions.

Degradation and adsorption of pesticides were important factors in both studies (Section 3.3). This study found degradation rates particularly critical for *Imidacloprid* and *Thiamethoxam* in P1 and P2, while Zhou et al. (2024) reported similar findings for other pesticides. Adsorption was also key, especially for *Chlorantraniliprole* and *Methoxyfenozide*.

Both this study and Zhou et al. (2024) underscore the critical role of soil texture in influencing model parameters and water flow and pesticide transport (Section 3.2 and Section 3.4). Sandier profiles, like P2, exhibit a higher saturated hydraulic conductivity ($K_s$), leading to faster water movement. In contrast, clay-rich soils as found at P1 have lower $K_s$, slowing the water movement. Cemented duripans in some profiles (P1 and P3) further reduced $K_s$, creating barriers to water infiltration. The sandier P2 profile had the highest groundwater recharge efficiency and shortest travel times, leading to more pesticide leaching, which was consistent across both studies.

A major strength of this study is its use of parameter uncertainty analysis through Bayesian methods, which offers a more comprehensive approach than particle swarm optimization (PSO) in Zhou et al. (2024). While PSO can provide uncertainty estimates by analyzing variability within the swarm, Bayesian analysis directly estimates the full posterior distribution of parameters, capturing a broader range of possible values and interactions. This provides a deeper understanding of how variations in pesticide properties affect model predictions (as shown in the range of pesticide mass balance components in Table 3), enhancing risk assessment of pesticide leaching and informing groundwater management under Ag-MAR practices.

### 4.2 Site-specific transport behaviors

The study revealed that both the maximum transport depths (MTDs) and relative differences in the maximum transport depths (RMTDs) between the Ag-MAR and Rainfall scenarios varied significantly across profiles (Figs. 5, 6, and 7; Table 5). In Profile P2, MTDs increased significantly from the Rainfall to Ag-MAR scenarios, rising from approximately 7.69–8.15 m under Rainfall to 17.86 m to 18.17 m under Ag-MAR across all pesticides, reflecting a substantial deepening of pesticide transport under high infiltration rates. The deeper transport observed in Profile P2 can be attributed to its high sand content (84%), which promotes faster water infiltration and deeper movement of pesticides. However, Profiles P1 and

P3, which contain more fine-textured soils in the shallow vadose zone, exhibited lower MTDs due to slower water flow.

Under the Rainfall scenario, Layers 6 (2.5–5 m) and 7 (5–20 m) acted as natural capillary barriers, slowing the downward movement of water and pesticides. This is because the transition from fine-textured layers to coarser ones created a hydraulic discontinuity, impeding water infiltration at these depths. The presence of capillary barriers under drier conditions allowed water to accumulate in the upper layers, reducing the transport of pesticides into deeper zones. However, under the Ag-MAR scenario, the large hydraulic gradients caused infiltration dynamics to be controlled by soil texture and hydraulic conductivity, with coarse layers promoting faster and deeper transport of water and pesticides. This distinction is critical for designing effective Ag-MAR strategies to minimize groundwater contamination risks, particularly in regions with variable soil textures.

### 4.3 Pesticide-specific transport behaviors

The transport behaviors of the four pesticides varied significantly in both absolute MTDs and RMTDs, highlighting the influence of pesticide properties on their movement through the vadose zone (Figs. 5, 6, and 7; Table 5).

*Methoxyfenozide* consistently exhibited the smallest MTDs across all profiles, such as 7.64 ± 1.49 m under Rainfall and 16.66 ± 4.31 m under Ag-MAR in P1. However, it showed the largest RMTDs, ranging from 123.6% ± 47.8% in P1 to 159.4% ± 53.5% in P3. This suggests that *Methoxyfenozide*, due to its low mobility and high persistence (discussed in Section 3.1), is more likely to be transported to deep soil layers during intensive flooding like Ag-MAR.

In contrast, *Thiamethoxam* generally exhibited the largest MTDs and smaller RMTDs across profiles. For example, its MTDs reached 8.15 ± 1.55 m under Rainfall and 18.10 ± 3.44 m under Ag-MAR in P2, with RMTDs ranging from 116.6% ± 42.9% in P1 to 130.3% ± 39.4% in P2. These results indicate that *Thiamethoxam*'s high mobility allows it to consistently reach deeper layers under both scenarios, resulting in smaller relative differences in transport depths between Rainfall and Ag-MAR scenarios.

The variability in both MTDs and RMTDs across the four pesticides highlights the importance of considering soil textures, hydraulic conditions, and pesticide properties when assessing groundwater contamination risks. *Methoxyfenozide* poses a higher risk of deep transport under Ag-MAR due to its large RMTDs, while *Thiamethoxam*, despite having the largest absolute MTDs, shows smaller relative increases during Ag-MAR due to its greater mobility. Understanding these dynamics is crucial for designing effective Ag-MAR management strategies to mitigate pesticide leaching risks.

**4.4 Limitations of this study**

Several site-specific and analytical constraints influenced the modeling results presented in this study. First, the bromide or pesticide samples were not taken at the exact same locations as the soil sensors, installed at a maximum of 3 meters apart. Pesticide sampling required collection of 1L pore water samples, which may have originated from a relatively large area of influence since it was collected with a high-capacity suction lysimeter over a 4–6-hour time window. Pesticide concentrations thus may not accurately represent soil water at a particular location and time.

Second, we employed a 1D model to simulate water flow and pesticide transport in the vadose zone primarily due to the vertical nature of the flow at our study site. The flooded recharge plot covered an area of 32,376 $m^2$ (approximately 100 m × 320 m), which is significantly larger than the 2.5 m soil profile depth. Given the uniform water application at the surface, the dominant flow pathway is expected to be vertical infiltration through the vadose zone. Therefore, the assumption of predominantly vertical flow is reasonable for this study. However, we assumed the groundwater table remained at 70 m during the entire experiment period. Groundwater levels are influenced by factors such as pumping drawdown and recharge mounds, which lead to lateral groundwater flow may cause variations and deviate from the constant 70 m assumption. Therefore, while our 1D model captures vertical transport through the vadose zone, a 2D/3D model would better evaluate broader regional groundwater quality impacts.

Third, in this study, the measured BTCs of bromide were used to calibrate the soil hydraulic and basic solute transport parameters ($\lambda$) and then used in the subsequent pesticide transport parameter optimization. This means that bromide and pesticide transport/reaction parameters were determined independently. As a result, the optimized dispersivities derived from bromide breakthrough curves (BTCs) may not be suitable for pesticides. Consequently, simultaneously improving the model performance for bromide and pesticides BTCs is challenging (Table S1). For instance, one study conducted the Morris sensitivity analysis simultaneously for water flow, nonreactive tracer, and reactive solute transport parameters for each reactive solute (Gatel et al., 2019). They found that soil hydraulic parameters were more influential than adsorption parameters in determining the Nash-Sutcliffe efficiencies (NSEs) of output solute fluxes. The authors recommended selecting the same set of parameters from the sensitivity analysis results that yielded the best NSE values for output flux simulations across all solutes, which significantly improved output solute flux simulation.

Fourth, the omission of preferential flow and transport and kinetic adsorption (a.k.a. physical and chemical nonequilibrium), often difficult to observe at the point scale (Vogel, 2019), makes it more challenging to accurately quantify pesticide fate and transport and its potential groundwater contamination risk (Jarvis, 2007). The earlier arrival and much narrower shapes of observed bromide BTCs or earlier arrival of observed pesticides BTCs compared to those simulated at P2 and P3 may be caused by preferential flow/transport (i.e., physical nonequilibrium) (Haws et al., 2005). In addition, we considered only linear adsorption, which requires fewer input parameters, while much research shows that nonlinear adsorption is more appropriate in some cases (Cheviron and Coquet, 2009). Model performance was worse for BTCs of *Methoxyfenozide* and at P2, which may be related to the omission in this study of potential kinetic adsorption (i.e., chemical nonequilibrium) since the rapid water flow during intensive flooding makes it more difficult to reach equilibrium adsorption (Dusek et al., 2015).

Fifth, the soil hydraulic parameters in the deep unsaturated zone were generated from typical 12 soil textural classes of the USDA textural triangle. In addition, since no measured adsorption and degradation coefficients were available in this study, they were neglected for the deep unsaturated zone (2.5-70 m). These simple treatments might bias the model results.

# 5 Conclusions

By integrating field observations, HYDRUS-1D modeling, and a Bayesian probabilistic approach, we analyzed the transport of four pesticides—*Imidacloprid*, *Thiamethoxam*, *Chlorantraniliprole*, and *Methoxyfenozide* in three (P1, P2, P3) deep (70 m) unsaturated zones characterized by varying textures in response to large water applications (1.2 $m^3/m^2$) for intentional groundwater recharge (agricultural managed aquifer recharge - Ag-MAR).

The results demonstrate that soil texture significantly controls the maximum transport depths (MTDs) of pesticides. Profiles P1 and P3, characterized by fine-textured soils in the shallow vadose zone, exhibited lower MTDs compared to Profile P2, which contained the highest sand content. Under natural rainfall conditions, capillary barriers formed by fine-textured layers between 2.5 and 20 meters depth effectively slowed water and pesticide infiltration. However, during Ag-MAR, the high-pressure infiltration overcame these barriers, pushing water and dissolved pesticides deeper into the vadose zone. This indicates that under large-scale recharge practices, subsurface heterogeneity must be carefully considered in site selection to manage the risks of pesticide leaching into groundwater.

The transport behavior of individual pesticides varied based on their properties. *Methoxyfenozide* exhibited the smallest absolute MTDs but posed the highest risk of deep transport under Ag-MAR due to its low mobility and persistence. Its relative maximum transport depth (RMTD) increased significantly during Ag-MAR, particularly in Profile P3, where it nearly tripled compared to the Rainfall scenario. In contrast, Thiamethoxam consistently displayed the deepest absolute MTDs across all profiles due to its high mobility, with relatively small RMTD increases between Rainfall and Ag-MAR scenarios. These contrasting behaviors highlight the importance of considering pesticide-specific properties when assessing the potential for groundwater contamination under recharge practices.

Overall, this study provides practical recommendations for managing pesticide leaching risks during Ag-MAR. Site selection should prioritize areas with fine-textured soils to minimize deep pesticide transport. Additionally, the timing and type of pesticide applications should be carefully managed, especially for persistent pesticides like *Methoxyfenozide* that pose a higher risk of reaching groundwater during recharge events. Future research should further explore preferential flow and nonlinear adsorption processes to improve model accuracy and better predict pesticide fate in the deep vadose zone.

## Acknowledgments

We acknowledge Mr. Don Cameron from Terranova Ranch for his support in collecting original data. Thanks to Dr. Sakiur Rahman from the University of California, Riverside, for his useful suggestions. This work was partially funded by USDA NIFA (Award # 2021-68012-35914), USDA NRCS (grant no NR203A750023C017), the Gordon and Betty Moore Foundation (grant no. 7975), and the California Department of Pesticide Regulation (Agreement 17-C0099).

## References

Behroozmand, A.A., Auken, E., Knight, R., 2019. Assessment of Managed Aquifer Recharge Sites Using a New Geophysical Imaging Method. Vadose Zone Journal 18(1), 13. https://doi.org/10.2136/vzj2018.10.0184.

Bexfield, L.M., Belitz, K., Lindsey, B.D., Toccalino, P.L., Nowell, L.H., 2021. Pesticides and Pesticide Degradates in Groundwater Used for Public Supply across the United States: Occurrence and Human-Health Context. Environ. Sci. Technol. 55(1), 362-372. https://doi.org/10.1021/acs.est.0c05793.

Brunetti, G., Šimůnek, J., Wöhling, T., Stumpp, C., 2023. An in-depth analysis of Markov-Chain Monte Carlo ensemble samplers for inverse vadose zone modeling. Journal of Hydrology 624, 24. https://doi.org/10.1016/j.jhydrol.2023.129822.

Brunetti, G., Stumpp, C., Šimůnek, J., 2022. Balancing exploitation and exploration: A novel hybrid global-local optimization strategy for hydrological model calibration. Environ. Modell. Softw. 150, 11. https://doi.org/10.1016/j.envsoft.2022.105341.

Celia, M.A., Bouloutas, E.T., Zarba, R.L., 1990. A GENERAL MASS-CONSERVATIVE NUMERICAL-SOLUTION FOR THE UNSATURATED FLOW EQUATION. Water Resour. Res. 26(7), 1483-1496. https://doi.org/10.1029/WR026i007p01483.

Cheviron, B., Coquet, Y., 2009. Sensitivity Analysis of Transient-MIM HYDRUS-1D: Case Study Related to Pesticide Fate in Soils. Vadose Zone Journal 8(4), 1064-1079. https://doi.org/10.2136/vzj2009.0023.

de Vries, J.J., Simmers, I., 2002. Groundwater recharge: an overview of processes and challenges. Hydrogeol. J. 10(1), 5-17. https://doi.org/10.1007/s10040-001-0171-7.

Dillon, P., Pavelic, P., Page, D., Beringen, H., Ward, J., 2009. Managed aquifer recharge.

Dillon, P., Stuyfzand, P., Grischek, T., Lluria, M., Pyne, R.D.G., Jain, R.C., Bear, J., Schwarz, J., Wang, W., Fernandez, E., Stefan, C., Pettenati, M., van der Gun, J., Sprenger, C., Massmann, G., Scanlon, B.R., Xanke, J., Jokela, P., Zheng, Y., Rossetto, R., Shamrukh, M., Pavelic, P., Murray, E., Ross, A., Valverde, J.P.B., Nava, A.P., Ansems, N., Posavec, K., Ha, K., Martin, R., Sapiano, M., 2019. Sixty years of global progress in managed aquifer recharge. Hydrogeology Journal 27(1), 1-30. https://doi.org/10.1007/s10040-018-1841-z.

Dusek, J., Dohnal, M., Snehota, M., Sobotkova, M., Ray, C., Vogel, T., 2015. Transport of bromide and pesticides through an undisturbed soil column: A modeling study with global optimization analysis. J. Contam. Hydrol. 175, 1-16. https://doi.org/10.1016/j.jconhyd.2015.02.002.

FAO, 2021. Pesticides use, pesticides trade and pesticides indicators. Global, regional and country trends, 1990–2019. FAOSTAT Anal Brief Ser No 29 Rome 22.

Gatel, L., Lauvernet, C., Carluer, N., Weill, S., Tournebize, J., Paniconi, C., 2019. Global evaluation and sensitivity analysis of a physically based flow and reactive transport model on a laboratory experiment. Environ. Modell. Softw. 113, 73-83. https://doi.org/10.1016/j.envsoft.2018.12.006.

Gelhar, L.W., Welty, C., Rehfeldt, K.R., 1992. A CRITICAL-REVIEW OF DATA ON FIELD-SCALE DISPERSION IN AQUIFERS. Water Resources Research 28(7), 1955-1974. https://doi.org/10.1029/92wr00607.

Gleeson, T., Wada, Y., Bierkens, M.F.P., van Beek, L.P.H., 2012. Water balance of global aquifers revealed by groundwater footprint. Nature 488(7410), 197-200. https://doi.org/10.1038/nature11295.

Goebel, M., Knight, R., 2021. Recharge site assessment through the integration of surface geophysics and cone penetrometer testing. Vadose Zone Journal 20(4), 18. https://doi.org/10.1002/vzj2.20131.

Goodman, J., Weare, J., 2010. Ensemble samplers with affine invariance. Communications in applied mathematics and computational science 5(1), 65-80.

Haws, N.W., Rao, P.S.C., Šimůnek, J., Poyer, I.C., 2005. Single-porosity and dual-porosity modeling of water flow and solute transport in subsurface-drained fields using effective field-scale parameters. Journal of Hydrology 313(3-4), 257-273. https://doi.org/10.1016/j.jhydrol.2005.03.035.

Isch, A., Montenach, D., Hammel, F., Ackerer, P., Coquet, Y., 2019. A Comparative Study of Water and Bromide Transport in a Bare Loam Soil Using Lysimeters and Field Plots. Water 11(6), 25. https://doi.org/10.3390/w11061199.

Jarvis, N.J., 2007. A review of non-equilibrium water flow and solute transport in soil macropores: principles, controlling factors and consequences for water quality. Eur. J. Soil Sci. 58(3), 523-546. https://doi.org/10.1111/j.1365-2389.2007.00915.x.

Jasechko, S., Seybold, H., Perrone, D., Fan, Y., Shamsudduha, M., Taylor, R.G., Fallatah, O., Kirchner, J.W., 2024. Rapid groundwater decline and some cases of recovery in aquifers globally. Nature 625(7996), 37. https://doi.org/10.1038/s41586-023-06879-8.

Köhne, J.M., Köhne, S., Mohanty, B.P., Šimůnek, J., 2004. Inverse mobile-immobile modeling of transport during transient flow: Effects of between-domain transfer and initial water content. Vadose Zone Journal 3(4), 1309-1321. https://doi.org/10.2113/3.4.1309.

Köhne, J.M., Köhne, S., Šimůnek, J., 2009. A review of model applications for structured soils: b) Pesticide transport. J. Contam. Hydrol. 104(1-4), 36-60. https://doi.org/10.1016/j.jconhyd.2008.10.003.

Konikow, L.F., 2011. Contribution of global groundwater depletion since 1900 to sea-level rise. Geophysical Research Letters 38, 5. https://doi.org/10.1029/2011gl048604.

la Cecilia, D., Dax, A., Ehmann, H., Koster, M., Singer, H., Stamm, C., 2021. Continuous high-frequency pesticide monitoring to observe the unexpected and the overlooked. Water Res. X 13, 11. https://doi.org/10.1016/j.wroa.2021.100125.

Levintal, E., Kniffin, M.L., Ganot, Y., Marwaha, N., Murphy, N.P., Dahlke, H.E., 2023. Agricultural managed aquifer recharge (Ag-MAR)-a method for sustainable groundwater management: A review. Crit. Rev. Environ. Sci. Technol. 53(3), 291-314. https://doi.org/10.1080/10643389.2022.2050160.

Liang, J.J., Qin, A.K., Suganthan, P.N., Baskar, S., 2006. Comprehensive learning particle swarm optimizer for global optimization of multimodal functions. IEEE Trans. Evol. Comput. 10(3), 281-295. https://doi.org/10.1109/tevc.2005.857610.

Mualem, Y., 1976. A new model for predicting the hydraulic conductivity of unsaturated porous media. Water Resources Research 12(3), 513-522. https://doi.org/10.1029/WR012i003p00513.

Pepin, K., Knight, R., Goebel-Szenher, M., Kang, S., 2022. Managed aquifer recharge site assessment with electromagnetic imaging: Identification of recharge flow paths. Vadose Zone Journal 21(3), 13. https://doi.org/10.1002/vzj2.20192.

Perzan, Z., Osterman, G., Maher, K., 2023. Controls on flood managed aquifer recharge through a heterogeneous vadose zone: hydrologic modeling at a site characterized with surface geophysics. Hydrology and Earth System Sciences 27(5), 969-990. https://doi.org/10.5194/hess-27-969-2023.

Riah, W., Laval, K., Laroche-Ajzenberg, E., Mougin, C., Latour, X., Trinsoutrot-Gattin, I., 2014. Effects of pesticides on soil enzymes: a review. Environ. Chem. Lett. 12(2), 257-273. https://doi.org/10.1007/s10311-014-0458-2.

Rooney, D.J., Brown, K.W., Thomas, J.C., 1998. The effectiveness of capillary barriers to hydraulically isolate salt contaminated soils. Water Air Soil Pollut. 104(3-4), 403-411. https://doi.org/10.1023/a:1004966807950.

Schaap, M.G., Bouten, W., 1996. Modeling water retention curves of sanely soils using neural networks. Water Resources Research 32(10), 3033-3040. https://doi.org/10.1029/96wr02278.

Schübl, M., Stumpp, C., Brunetti, G., 2022. A Bayesian perspective on the information content of soil water measurements for the hydrological characterization of the vadose zone. Journal of Hydrology 613, 16. https://doi.org/10.1016/j.jhydrol.2022.128429.

Sim, J.X.F., Doolette, C.L., Vasileiadis, S., Drigo, B., Wyrsch, E.R., Djordjevic, S.P., Donner, E., Karpouzas, D.G., Lombi, E., 2022. Pesticide effects on nitrogen cycle related microbial functions and community composition. Science of the Total Environment 807, 12. https://doi.org/10.1016/j.scitotenv.2021.150734.

Šimůnek, J., Brunetti, G., Jacques, D., van Genuchten, M.T., Sejna, M., 2024. Developments and applications of the HYDRUS computer software packages since 2016. Vadose Zone J. 23(4), 29. https://doi.org/10.1002/vzj2.20310.

Šimůnek, J., Hopmans, J.W., 2002. 1.7 parameter optimization and nonlinear fitting. Methods of Soil Analysis: Part 4 Physical Methods 5, 139-157.

Šimůnek, J., van Genuchten, M.T., Sejna, M., 2016. Recent Developments and Applications of the HYDRUS Computer Software Packages. Vadose Zone J. 15(7), 25. https://doi.org/10.2136/vzj2016.04.0033.

van Genuchten, M.T., 1980. A closed-form equation for predicting the hydraulic conductivity of unsaturated soils. Soil Science Society of America Journal 44(5), 892-898. https://doi.org/10.2136/sssaj1980.03615995004400050002x.

Vereecken, H., Weynants, M., Javaux, M., Pachepsky, Y., Schaap, M.G., van Genuchten, M.T., 2010. Using Pedotransfer Functions to Estimate the van Genuchten-Mualem Soil Hydraulic Properties: A Review. Vadose Zone Journal 9(4), 795-820. https://doi.org/10.2136/vzj2010.0045.

Vogel, H.J., 2019. Scale Issues in Soil Hydrology. Vadose Zone Journal 18(1), 10. https://doi.org/10.2136/vzj2019.01.0001.

Wosten, J.H.M., van Genuchten, M.T., 1988. Using texture and other soil properties to predict the unsaturated soil hydraulic functions. Soil Sci. Soc. Am. J. 52(6), 1762-1770.

Zhou, T., Šimůnek, J., Braud, I., Nasta, P., Brunetti, G., Liu, Y., 2022. The impact of evaporation fractionation on the inverse estimation of soil hydraulic and isotope transport parameters. Journal of Hydrology 612, 128100. https://doi.org/https://doi.org/10.1016/j.jhydrol.2022.128100.

Zhou, T.T., Ruud, N., Simunek, J., Brunetti, G., Levintal, E., García, C.P., Dahlke, H.E., 2024. The impact of managed aquifer recharge on the fate and transport of pesticides in agricultural soils. Water Res. 267, 12. https://doi.org/10.1016/j.watres.2024.122442.